EPJ Web of Conferences **265**, 00031 (2022) https://doi.org/10.1051/epjconf/202226500031
Multi-line Diagnostics of the Interstellar Medium

Fragmentation and disk formation in high-mass star formation: The IRAM large program CORE

Henrik Beuther[1,*], *Caroline* Gieser[1], *Aida* Ahmadi[2], *Sümeyye* Suri[3], *Jan Martin* Winters[4], *Joe* Mottram[1], and the CORE team[**]

[1]Max Planck Institute for Astronomy, Königstuhl 17, 69117 Heidelberg, Germany
[2]Leiden Observatory, Leiden University, PO Box 9513, 2300 RA Leiden, The Netherlands
[3]Department of Astrophysics, University of Vienna, Türkenschanzstrasse 17, 1180 Vienna, Austria
[4]IRAM, 300 rue de la Piscine, Domaine Universitaire de Grenoble, 38406 St.-Martin-d'Hères, France

Abstract. The IRAM CORE large program combines data from NOEMA and the IRAM 30 m telescope to study a diverse set of physical and chemical processes during the formation of high-mass stars. Here, we present a selected compilation of exciting results obtained during the survey.

1 Introduction

Some of the central questions in high-mass star formation research relate to the fragmentation and disk formation processes as well as the physical and chemical conditions during the formation of massive stars. To address these questions, we conducted the IRAM large program CORE "Fragmentation and disk formation in high-mass star formation" combining observations with the Northern Extended Millimeter Array (NOEMA) and the IRAM 30 m telescope. An introduction to the survey, its scope and initial results focusing on the 1.3 mm continuum emission can be found in [1]. In addition to the original CORE program targeting 20 high-mass protostellar objects, we extended the survey to earlier evolutionary stages via the CORE-extension project that targets two younger regions at the onset of high-mass star formation [2, 3].

2 Selected results

In the following, we will present some selected results corresponding to the important scientific topics studied within the CORE project. In addition to the studies comprising the entire CORE sample [1, 4] and Ahmadi et al. (in prep.), we also conducted a broad range of individual case studies to dissect the processes in individual sources at depth [5–11].

2.1 Fragmentation

Figure 1 presents the 1.3 mm continuum data of the entire CORE sample [1]. While the angular resolution varied roughly between 0.3 – 0.4″, here we show all regions converted to

*e-mail: beuther@mpia.de
**http://www.mpia.de/core

the same linear box size of $\sim 4 \times 10^4$ au. Already a visual inspection of the data shows a broad variety in fragmentation properties, from regions dominated by a single massive core to those that harbor up to 20 cores. Analyzing the core separations by means of a minimum-spanning-tree analysis, the CORE regions are consistent with thermal Jeans fragmentation. Nevertheless, the diversity of fragments per region indicates that other processes are likely at play. Variations of the initial density profiles and/or magnetic field could cause the diversity of fragmentation properties. These questions are currently investigated by ongoing follow-up projects.

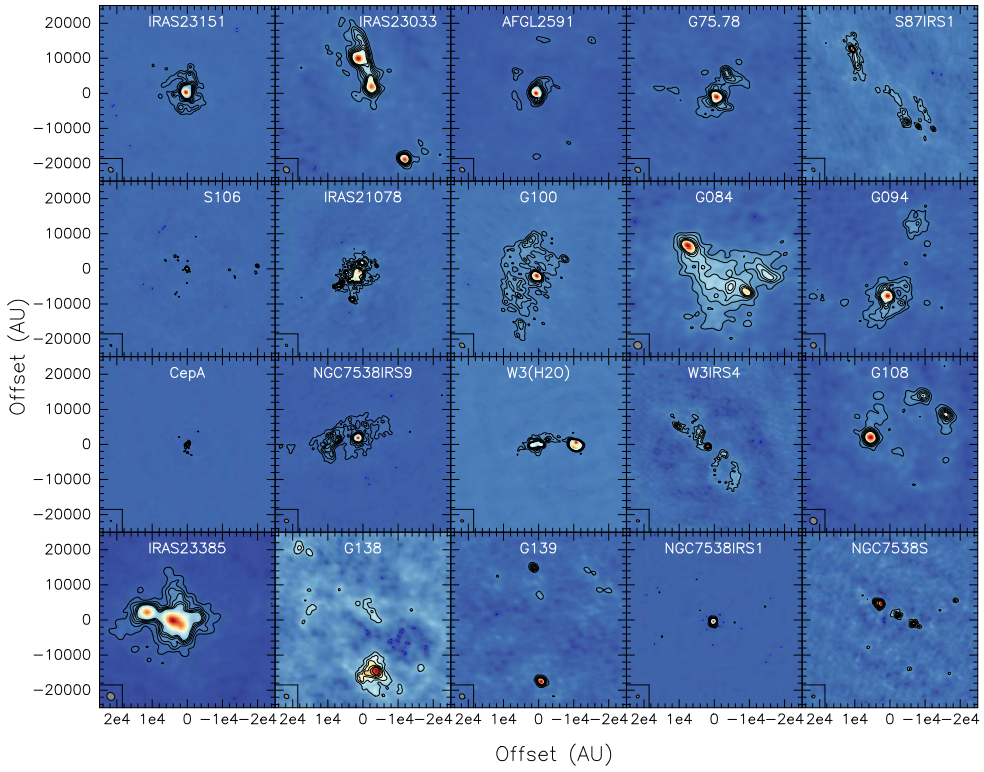

Figure 1. Compilation of 1.3 mm continuum images of the CORE sample converted to linear resolution elements [1]. The contouring is in 4σ steps. The sources are labeled in each panel, and the synthesized beam is shown at the bottom-left of each panel.

2.2 Disk formation

While protostellar disks are well studied around low-mass protostars, they are significantly less explored in the high-mass regime. Within the CORE project with linear resolution elements typically on the order of ~1000 au, we usually cannot resolve the innermost disks. But nevertheless, we can study the rotational properties of the larger-scale disk-like structures. From the 20 CORE regions, we identify in 12 of them rotational motions perpendicular to the outflows (Ahmadi et al. in prep.). At high angular resolution, some even fragment into multiple disk-sources like W3(H_2O) [5]. Fitting the CH_3CN data with XCLASS, we can derive temperature maps of the regions. Employing furthermore the column density information

from the 1.3 mm continuum data and assuming Keplerian rotation, we can infer Toomre Q stability maps. Figure 2 (left) presents the corresponding Toomre Q map of the multiple system W3(H_2O) [5]. While the Q values are high close to the protostars, in the outskirts of the region we find decreasing Q values, in the west coinciding with an additional mm continuum peak. This is a strong indication for fragmentation on disks scales.

For one region, AFGL2591, we have even higher-resolution data at 0.19″ resolution with NOEMA at 843 μm wavelengths (Fig. 2 right). These data allow us to spatially resolve the fragmenting disk [11]. Combining this disk fragmentation with the thermal Jeans fragmentation investigated in section 2.1, we can differentiate between two fragmentation modes: core fragmentation on cluster scales and disk fragmentation on scales of individual multiple systems.

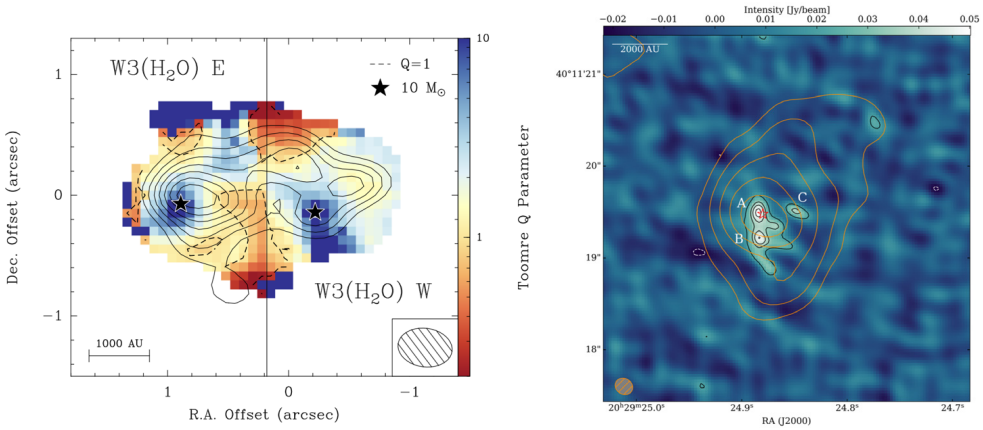

Figure 2. *Left:* Toomre Q map of the W3(H_2O) region [5]. The contours present the 1.3 mm continuum data, and the stars mark the locations of the two assumed 10 $M_\odot$ protostars. *Right:* Resolved disk-structure in AFGL2591 [11]. The color-scale shows the 843 μm continuum emission at 0.19″ resolution whereas the orange contours present the previous 1.3 mm continuum emission at 0.4″ resolution. The letters mark the three main structures and the red star marks the position of the central protostar assumed to coincide with the 1.3 mm continuum peak.

2.3 Physical properties

What are the physical properties, in particular the density and temperature structures of high-mass star-forming regions on small core scales? While density $\rho \propto r^{-p}$ (left) and temperature profiles $T \propto r^{-q}$ have been predicted since decades [12, 13], no statistical analysis of these structural parameters existed on scales of several thousand au around forming high-mass protostars. Within the CORE project, we now derived the temperature as well as the density structures of a large sample of cores.

While temperatures are derived from spectral line fitting, in particular the H_2CO lines in the 1 mm band, the situation is more difficult for the density structures since the derivation relies on the continuum emission. In contrast to the line data where complementary short spacing observations with the 30 m telescope exist, and hence all spatial structures are covered, the continuum data suffer from missing flux. Therefore, the continuum data were fitted directly in the uv-plane. Using the derived slopes of the uv-intensity fits, and adding-in the

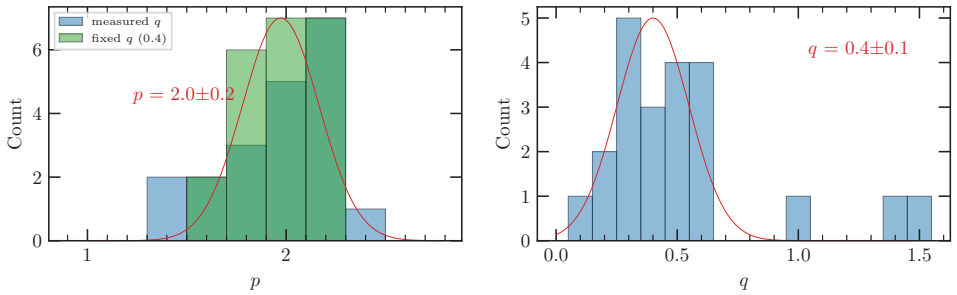

Figure 3. Histograms of the power-law distributions of the density $\rho \propto r^{-p}$ (left) and temperature structure $T \propto r^{-q}$ (right) derived on core scales [4]. The green and blue histograms in the left panel correspond to the density coefficients assuming fixed or measured q.

temperature information, we can infer the density structures. We apply this analysis to in total 22 fragmented cores. All details can be found in [4].

Figure 3 presents the histograms of all derived power-law indices for the density as well as temperature structures [4]. While the density power-law index ranges around 2, the temperature power-law distribution peaks around 0.4. These mean values agree extremely well with theoretical models of star-forming cores heated from an internal protostar. It is exciting to see that long-standing predictions can finally be confirmed by observations.

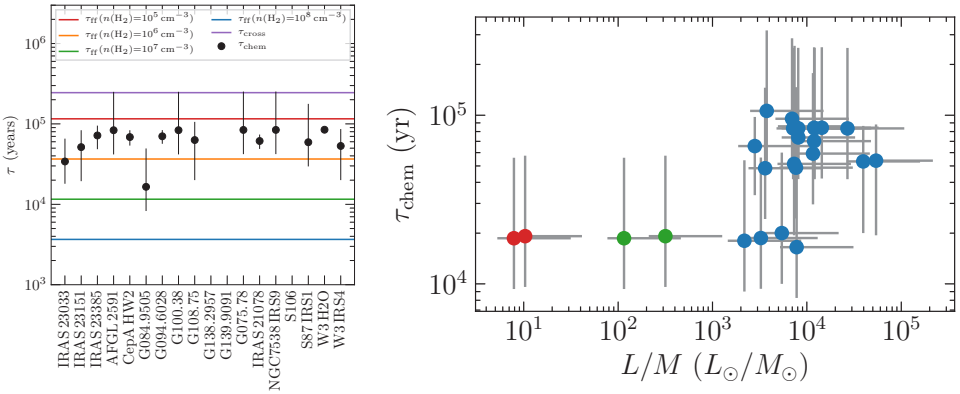

Figure 4. Chemical timescales derived from the CORE and CORE-extension projects [3, 4]. The left panel shows the timescales for all sources of the original CORE sample in comparison to crossing and free-fall times. The right panel presents the chemical time-scales of both samples compared to the luminosity-over-mass ratio L/M as independent evolutionary stage tracer. Blue markers are the original CORE sources whereas green and red markers correspond to the CORE-extension sources.

2.4 Chemical evolution

The broad bandpass of the IRAM observations allows us to also investigate the chemical properties of the regions in detail. As a first step, Gieser et al. [3, 4] fitted all the spectral lines with XCLASS [14] and derived the gas column densities and abundances. Then, using

the physical-chemical modeling tools MUSCLE [15–17], the chemical properties could be investigated in detail [3, 4].

One of the outcomes are chemical timescales of all regions. Figure 4 presents in the left panel the chemical timescales for the original CORE sample, and they are all in the range of several ten-thousand years. These timescales are much shorter than the dynamical timescales of the parental gas clumps, but they are in rough agreement with the free-fall times at densities between 10^5 and 10^6 cm^{-3}.

Adding in the information derived from a similar analysis for the younger regions of the CORE-extension study, Gieser et al. find evidence that the chemical timescales are indeed correlating with other independent age indicators like the luminosity-over-mass ratio L/M [3]. While chemical timescales are notoriously prone to large error budgets, it is encouraging to see that these chemical times can be well used as independent age indicator.

2.5 Dynamical cloud and star formation

Within the CORE-extension program, we targeted two younger regions in larger-scale mosaic observations. In addition to similar analysis as outlined above, these data also allow us to investigate the cloud formation processes. Figure 5 shows the DCO^+ 1st moment map and a position-velocity cut through the ISOSS23053 region. Interestingly, we find two well-separated velocity components that meet exactly at the location where most of the dense cores are identified in the 1.3 mm continuum emission. At core positions we measure velocity gradients as large as 50 km s^{-1}pc^{-1}. These are clear signatures of converging gas flows that appear to be conducive to trigger star formation at their interaction zone. More details can be found in [2, 3].

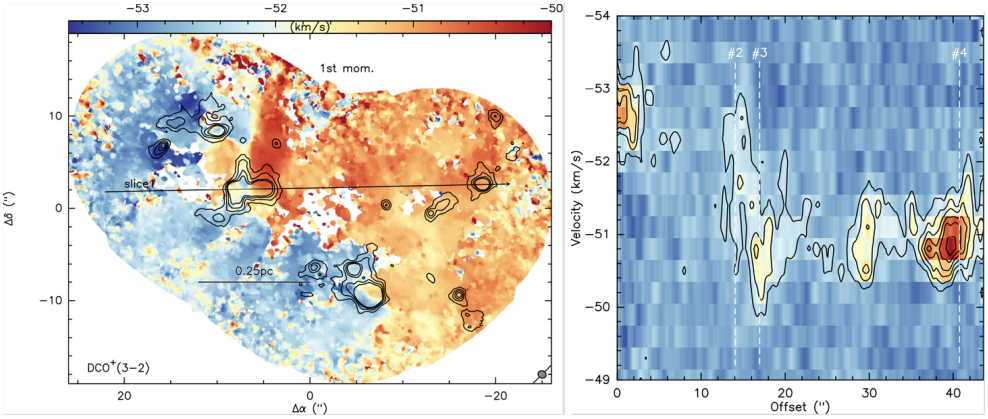

Figure 5. DCO^+(3–2) data towards ISOSS23053 [2]. The left panel shows in color-scale the DCO^+ 1st moment map and in contours the corresponding 1.3 mm continuum data. The right panel presents a position-velocity cut through the DCO^+ data cube along the marked slice in the left panel.

3 Summary and outlook

As outlined so far, the IRAM CORE program allowed us to derive exciting results for a broad range of physical and chemical questions in the field of star formation. Nevertheless, open questions remain. For example, the spectral setup in the 1 mm band did not cover many

important ground-state lines, also from deuterated species. We therefore started a CORE+ study at NOEMA (Gieser et al.), targeting the CORE regions in the 3 mm band. Furthermore, while 20+ regions in the CORE and CORE-extension studies are already a big leap compared to earlier studies, larger statistical studies are now possible. For example the ALMA large program ALMAGAL targets more than 1000 regions in various evolutionary stages in a similar spectral setup. These data will allow us to address many of the here discussed topics on statistical grounds. In addition to that, the advent of JWST will enable studies of the physical and chemical properties of high-mass protostars at mid-infrared wavelengths and will be truly complementary to the CORE program.

References

[1] H. Beuther, J.C. Mottram, A. Ahmadi, F. Bosco, H. Linz, T. Henning, P. Klaassen, J.M. Winters, L.T. Maud, R. Kuiper et al., A&A**617**, A100 (2018), 1805.01191
[2] H. Beuther, C. Gieser, S. Suri, H. Linz, P. Klaassen, D. Semenov, J.M. Winters, T. Henning, J.D. Soler, J.S. Urquhart et al., A&A**649**, A113 (2021), 2104.02420
[3] C. Gieser, H. Beuther, D. Semenov, S. Suri, J.D. Soler, H. Linz, J. Syed, T. Henning, S. Feng, T. Möller et al., A&A**657**, A3 (2022), 2110.01896
[4] C. Gieser, H. Beuther, D. Semenov, A. Ahmadi, S. Suri, T. Möller, M.T. Beltrán, P. Klaassen, Q. Zhang, J.S. Urquhart et al., A&A**648**, A66 (2021), 2102.11676
[5] A. Ahmadi, H. Beuther, J.C. Mottram, F. Bosco, H. Linz, T. Henning, J.M. Winters, R. Kuiper, R. Pudritz, Á. Sánchez-Monge et al., A&A**618**, A46 (2018), 1808.00472
[6] F. Bosco, H. Beuther, A. Ahmadi, J.C. Mottram, R. Kuiper, H. Linz, L. Maud, J.M. Winters, T. Henning, S. Feng et al., A&A**629**, A10 (2019), 1907.04225
[7] R. Cesaroni, H. Beuther, A. Ahmadi, M.T. Beltrán, T. Csengeri, R. Galván-Madrid, C. Gieser, T. Henning, K.G. Johnston, P.D. Klaassen et al., A&A**627**, A68 (2019), 1905.11257
[8] C. Gieser, D. Semenov, H. Beuther, A. Ahmadi, J.C. Mottram, T. Henning, M. Beltran, L.T. Maud, F. Bosco, S. Leurini et al., A&A**631**, A142 (2019), 1910.05081
[9] J.C. Mottram, H. Beuther, A. Ahmadi, P.D. Klaassen, M.T. Beltrán, T. Csengeri, S. Feng, C. Gieser, T. Henning, K.G. Johnston et al., A&A**636**, A118 (2020)
[10] L. Moscadelli, H. Beuther, A. Ahmadi, C. Gieser, F. Massi, R. Cesaroni, Á. Sánchez-Monge, F. Bacciotti, M.T. Beltrán, T. Csengeri et al., A&A**647**, A114 (2021), 2102.04872
[11] S. Suri, H. Beuther, C. Gieser, A. Ahmadi, Á. Sánchez-Monge, J.M. Winters, H. Linz, T. Henning, M.T. Beltrán, F. Bosco et al., A&A**655**, A84 (2021), 2109.04751
[12] F.H. Shu, ApJ**214**, 488 (1977)
[13] R.B. Larson, MNRAS**145**, 271 (1969)
[14] T. Möller, C. Endres, P. Schilke, A&A**59**, A7 (2017), 1508.04114
[15] D. Semenov, F. Hersant, V. Wakelam, A. Dutrey, E. Chapillon, S. Guilloteau, T. Henning, R. Launhardt, V. Piétu, K. Schreyer, A&A**522**, A42 (2010), 1007.2302
[16] T. Gerner, H. Beuther, D. Semenov, H. Linz, T. Vasyunina, S. Bihr, Y.L. Shirley, T. Henning, A&A**563**, A97 (2014), 1401.6382
[17] T. Gerner, Y.L. Shirley, H. Beuther, D. Semenov, H. Linz, T. Albertsson, T. Henning, A&A**579**, A80 (2015), 1503.06594